Impact assessment of the polarization non-compliances discovered during J1 VIIRS prelaunch characterization: Impact on Ocean Environmental Data Records (EDR)

Gerhard Meister, Kevin Turpie
14 July 2014

EDRs considered: chlorophyll-a concentration, water-leaving radiances (or remote sensing reflectance)

Abstract

The NASA ocean team undertook an evaluation of the impact to ocean color data products of J1 VIIRS polarization characterization uncertainty and spectral properties. The evaluation involved a sensitivity analysis of the polarization correction to characterization error and a look at modeled spectral properties of J1 VIIRS polarization response. The results for highly stressing, but relatively unlikely, scenario for characterization error over open ocean and coastal waters caused small, but acceptable error in ocean color products. Thus, the reported characterization uncertainties are acceptable, although it is not clear what the larger polarization response of J1 VIIRS implies regarding correction performance, especially regarding the uncertainty of the polarization state of the Top-of-Atmosphere (TOA) radiance. Modeled spectral variation of band passes with change in polarization state showed band centers variation within 0.2 nm of the average case. Applying this band pass variation to spectra that are similar to Rayleigh or Blackbody sources produced small, but anti-correlated, variation in radiance. This suggests that when using a source that is spectrally different than Rayleigh, systematic effects stemming from spectral properties of J1 VIIRS polarization response could still lead to scan geometry dependent striping, even though the characterization measurements are within uncertainty requirements. Therefore correction coefficients derived from a characterization based on a Rayleigh-like source may be preferable to reduce striping. Further study will be required for the ocean data products to address these issues with flight data, but there is no obvious concern with the current waiver requested.

Introduction

The correction for the polarization response of the VIIRS instruments to measurement of Top-of-Atmosphere (TOA) radiance or reflectance is essential to calculating accurate ocean water-leaving radiance (or remote sensing reflectance), from which all traditional ocean color data products are derived. Without this correction, the ocean data products would show strong scan dependent biases and striping that would vary seasonally and hemi-spherically across the globe. Previous experience with MODIS Aqua showed that this can also impact global and synoptic trends, thus adversely affecting these products as climate data records.

The ocean color processing from both IDPS and NASA has the capability of apply this correction to the ocean products (NOAA EDRs or NASA Level-2 products, respectively) by applying the correction factor p_c, defined as

$$p_c = \frac{L_m}{L_t} \quad \text{Eq. 1}$$

where L_m and L_t are defined as the measured and true TOA radiance, respectively. For most scan angles, p_c can be calculated as

$$p_c = \frac{1}{1 - m_{12} Q_t / L_m - m_{13} U_t / L_m} \quad \text{Eq. 2}$$

where Q_t and U_t are the modeled Stokes Vector components of the TOA radiance associated with molecular scatter. For scan angles close to nadir, a matrix rotation is needed, as described by eq. 5 in Meister et al. (2005). This method has been employed for ocean color for a long time and experience with it is extensive. Gordon et al. (1997) originally developed this correction approach and its implementation for MODIS is practically identical to the VIIRS implementation (except of course for the values of the coefficients m_{12} and m_{13}, which are derived from the prelaunch characterization of the respective instruments).

The polarization response correction is applied to the TOA radiance during NOAA EDR or NASA Level-2 processing. Note that it is not applied during Level-1 processing, even though the TOA radiance is a NOAA Sensor Data Record (or NASA Level-1) product. The polarization characteristics of the TOA radiance must be known in order to apply the polarization correction to the input to the Level-2 product. The most important piece of information needed to derive the polarization characteristics of the TOA radiance is the amount of Rayleigh scattered light present. The Rayleigh amount is modeled using solar and view geometries and pressure information. Geometric information is routinely included in the SDR or Level-1 processing. Obtaining pressure information in a timely fashion can be rather challenging. However, even if the pressure information can be made available during SDR or Level-1 processing, the required code modifications would be substantial. Although it seems logical to apply the correction during SDR processing, implementation could be costly and challenges to product latency may make this impractical.

It has been generally accepted that the correction should work if the sensor polarization response is relatively small and has been characterized to within 0.5% uncertainty (i.e., within instrument requirements). However, although J1 VIIRS characterization uncertainty for polarization response has been claimed to be within this uncertainty threshold, the response observed for this sensor exceeded instrument requirements, and in some cases exceeded that of heritage sensors (especially at 551nm). Furthermore, it was apparent that changes in the spectral response across each band pass could further degrade the correction effectiveness. Therefore, a sensitivity analysis of a highly stressing scenario for characterization error was employed to determine whether the assumption that the characterization uncertainty was adequate and to evaluate the potential impact of apparent the spectral properties of the J1 VIIRS polarization response.

The impact of a greater response would be to magnify uncertainties in the actual correction method. For instance, the current correction method assumes that most or all TOA polarization can be attribute to molecular (i.e., Rayleigh) scattering of light. The effects of small, unknown causes of suppression or increase of TOA polarization would be magnified, perhaps large enough to become significant, by the much larger polarization response of J1 VIIRS. However, as we cannot estimate the size of these small effects *a priori*, we can only evaluate the quality of the flight data after launch for systematic effects. In the meanwhile, we must assume any such inaccuracies in the polarization correction method will remain small, even in the presence of the greater J1 VIIRS polarization response.

GMTCO_npp_d20120922_t0028043_e0029285_b04677

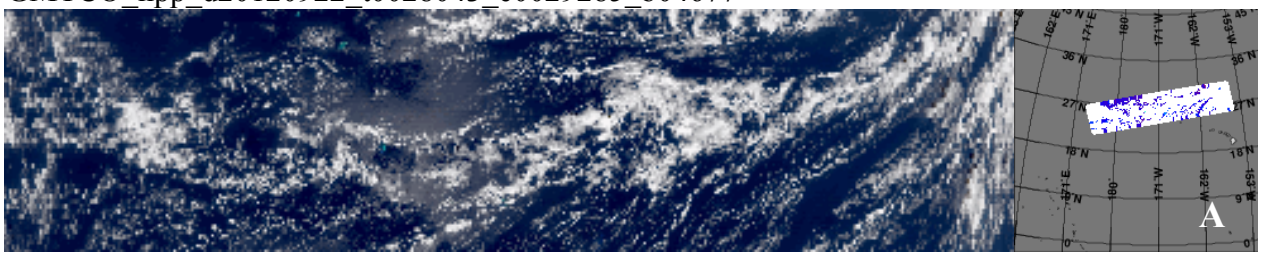

GMTCO_npp_d20140109_t1744402_e1746044_b11412

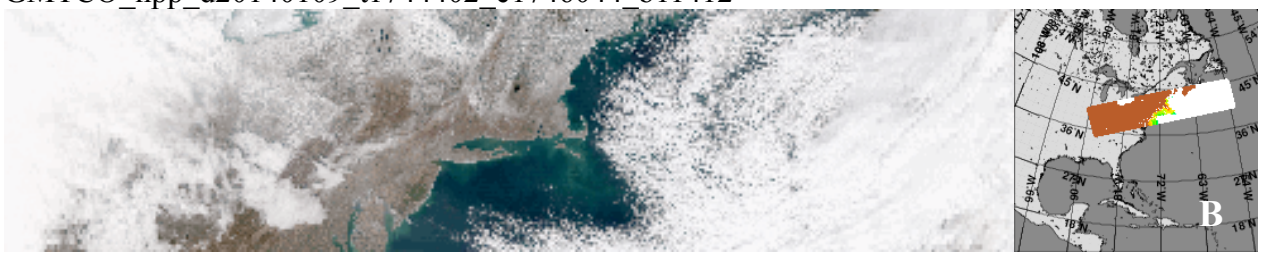

Figure 1 – NPP VIIRS scenes used for polarization characterization error sensitivity analysis. To scenes were evaluated to capture the extremes of surface conditions and scatter angles: A) Scene taken 22 September 2013 over the open Pacific Ocean, just northwest of Hawaii. B) Scene taken 9 January 2014 over the Atlantic Ocean along the coast of the northeastern USA.

Characterization Error Sensitivity Analysis

Approach

The data sets used for this analysis are two granules from NPP VIIRS, corrected for polarization: one granule from the open ocean, one from a coastal area (see Figure 1). These two granules cover two very different ocean color scenarios: the open ocean has high water-leaving radiances in the blue, and low radiances in the green, whereas for the coastal data it is typically the opposite. Therefore, we expect the relative impact of the uncertainty due to the polarization correction to be higher for the blue bands in the coastal data than in the open ocean data, and to be higher for the green bands in the open ocean data than in the coastal data. These granules were processed in the NASA GSFC Ocean color Data Processing System (ODPS) from NOAA Raw Data Records (RDR) to NASA Level-1 files, with solar calibration suppressed, using the Algorithm Development Library (ADL) developed for processing NPP data products. NASA solar calibration was then applied to the Level-1 granules and processed to Level-2 using the

SeaDAS software program. The Level-2 data files contained water-leaving radiance and chlorophyll-*a* concentration. The SeaDAS software was also set to include TOA radiance and components from the Stokes components.

The data were perturbed to simulate a large and relatively rare instance of error. This algorithm stressing error condition was based on the polarization response characterization uncertainties provided by in a report by the NASA VIIRS Calibration Support Team (VCST) (McIntire, 2014). The NPP VIIRS Stokes coefficients in the SeaDAS look-up tables were altered by an amount corresponding to this simulated error. The 'Total' uncertainty provided in the VCST report varies by band from 0.13% to 0.38%. Because it was not known how the simulated error was distributed between the Stokes components, the entire perturbation was applied to m_{12}, without loss of generality. Initially, the variation was applied in a spectrally coherent way (e.g., m_{12} was increased for all bands). This resulted in rather small variations of the ocean color products. It is well known that the current ocean color products used by NASA and NOAA are not as sensitive to spectrally coherent errors. Therefore, we decided to select the sign of the m_{12} perturbation, with the goal of maximizing the expected impact on the chlorophyll algorithm. The selected m_{12} perturbations are shown in Table 1. M4 has the opposite sign of M1-M3 (the chlorophyll algorithm is a ratio algorithm of the blue bands to the green M4 band), and M6 and M7 have opposite signs to increase the impact on the aerosol model selection.

Table 1: Modifications of the m_{12} parameter as evaluated in this study. Note that the above approach assumes that all the uncertainty is covered by the m_{12} parameter, and that the m_{13} parameter is perfect. It would be more realistic to assume that both parameters contribute to the total uncertainty. Unfortunately, this increases the number of possibilities that need to be evaluated tremendously. However, we do not expect that varying both m_{12} and m_{13} would lead to significantly different conclusions.

VIIRS band	**M1** (412 nm)	**M2** (443 nm)	**M3** (488 nm)	**M4** (551 nm)	**M5** (667 nm)	**M6** (748 nm)	**M7** (865 nm)
m_{12} change	-0.0038	-0.0014	-0.0020	0.0013	0.0019	-0.0014	0.0013

The two test granules were run both with the unperturbed correction parameters and the perturbed case of Table 1. We produced a full suite of TOA radiances, water-leaving radiances, and chlorophyll-a concentration, and then calculated the differences between the perturbed and the unperturbed cases.

Results

The TOA radiances differed by less than 0.2%, with the highest differences (very close to 0.2%) occurring for the M1 band (see Figure 2). This result was expected: the largest uncertainty provided by VCST was 0.38%, which would apply to completely linearly polarized light. The actual degree of polarization of the TOA radiance is usually less than 70%.

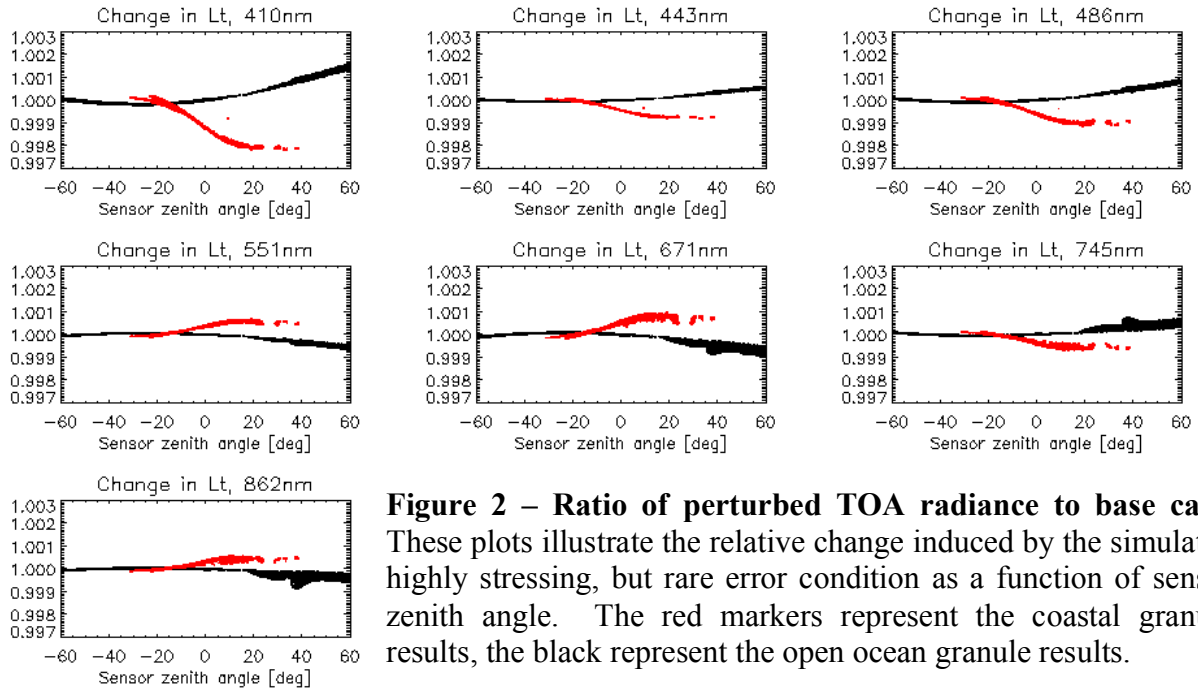

Figure 2 – Ratio of perturbed TOA radiance to base case. These plots illustrate the relative change induced by the simulated highly stressing, but rare error condition as a function of sensor zenith angle. The red markers represent the coastal granule results, the black represent the open ocean granule results.

For the open ocean granule, the water-leaving radiances were affected by less than 5% for the blue bands, more for green and red band. For the coastal granule, the 410 nm water-leaving radiance was affected most (up to 10%). Both the magnitude and the spectral dependence of the impact of the disturbance are in line with expectations.

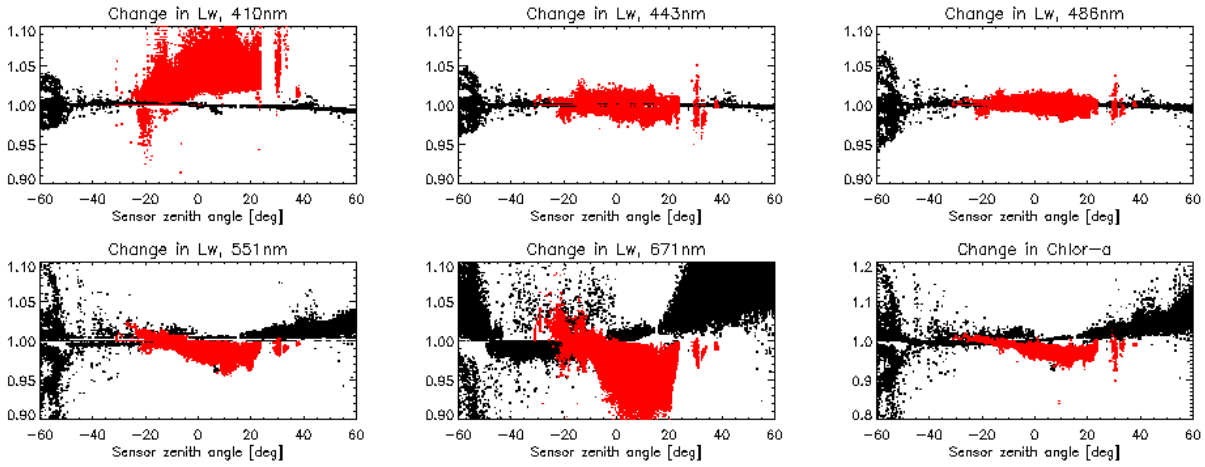

Figure 3 – Ratio of perturbed EDR or Level-2 products to base case. These plots illustrate the relative change induced by the simulated highly stressing, but rare error condition as a function of sensor zenith angle. The red markers represent the coastal granule results, the black represent the open ocean granule results.

For the open ocean granule, the chlorophyll-a concentration changes by more than 10% for less than 0.3% of the retrievals, and by 0.01 mg m^{-3} for less than 0.02% of the retrievals. For the coastal granule, chlorophyll-*a* concentration changes by more than 5% for less than 1.1% of the

retrievals (with no change larger than 10%), by 0.01 mg m^{-3} for ~70% of the retrievals, and by 0.1 mg m^{-3} for ~1% of the retrievals.

Evaluation of Spectral Effects

Approach

Spectral transmission over each J1 VIIRS band pass, for five detectors (1, 4, 8, 13, and 16), for five polarization states, and seven scan angles, was provided by a Raytheon model of J1 VIIRS using the Fred Optical Engineering Software (FRED®). This modeled transmission was evaluated to understand how changes the polarization state of incoming light would affect the measurements. First, the band centers were calculated as the centroid weighted by the modeled spectral transmission, which was mostly limited to the in-band region. Band centroids were tabulated by band, detector, scan angle, and polarization states (four polarization angles for linearly polarized light and an unpolarized case). These results can be found in Appendix A. Second, the spectral transmission curves were used to calculated a weighted average of radiance for a Rayleigh spectrum (i.e., $L_t \propto \lambda^{-4}$) and a 2300°K blackbody radiance spectrum (i.e., $2hc^2\lambda^{-5}/(e^{hc/\lambda kT}-1)$, where T=2300°K, h is Planck's constant, c is the speed of light *in vacuo*, and k is Boltzmann's constant). It is recognized that other source spectra were used during characterization, but those spectra were not readily available and it was instructive to see the

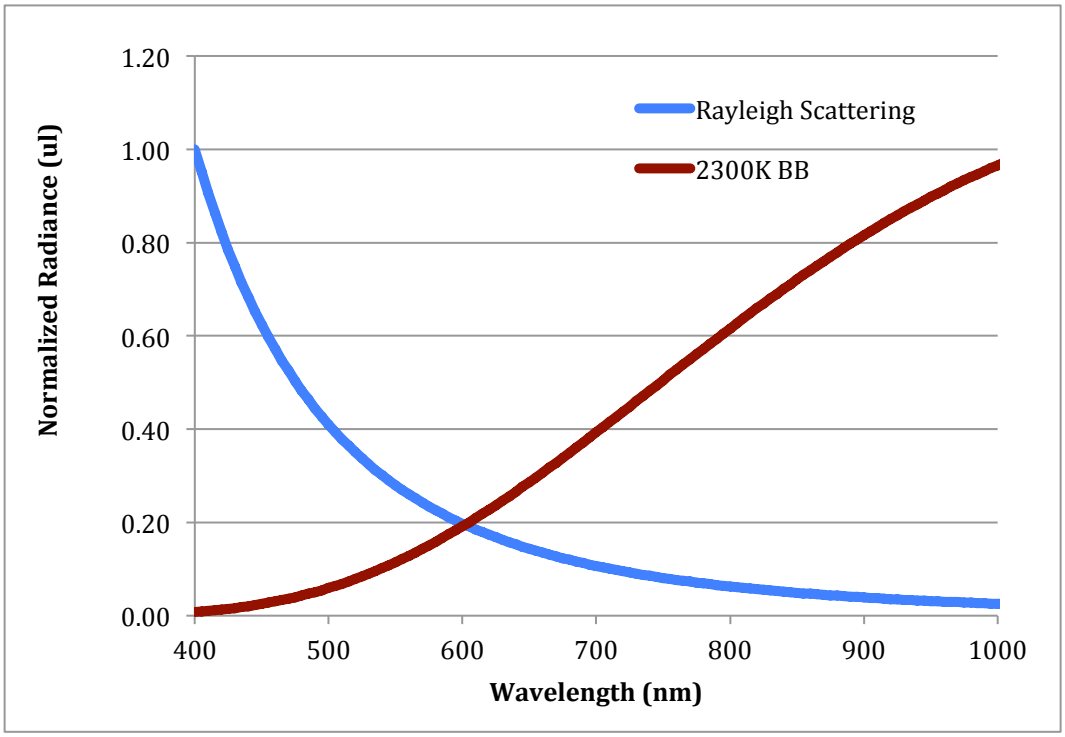

Figure 4 – Radiance spectra shapes for evaluation. Curves are normalized to the maximum over domain (blackbody spectrum maximum is not shown).

extreme cases offered by Rayleigh and blackbody spectra (see Figure 4). The resulting radiance values for both spectra were tabulated by band, detector, scan angle, and polarization state. The relative difference from the average radiance for each band was calculated (the average being

taken over detector, scan angle, and polarization state). The resulting relative percent differences are given in in Appendix B.

Results

The FRED® model predicts that the most significant variation in band centroid over detectors. This modeled spectral "smile" was seen to be largely symmetric for bands M2 through M7, with the highest (longest) wavelength being near detector 8 (i.e., the middle of the focal plane), but with slightly shorter wavelength centroid at detector 1 than detector 16 (thus it was an inverted "smile"). This slight asymmetry was much more pronounced for band M1, which had much more emphasis on detector 1 and the centroid peak was somewhere between detectors 4 and 8. The predicted variation of band center with detector was comparable to measured values for NPP VIIRS via observatory tests with Traveling Spectral Irradiance and Radiance Responsivity Calibrations Using Uniform Sources (T-SIRCUS) (Brown et al., 2006; McIntire et al., 2011; Guenther, 2012). The maximum variation of the smile was generally not greater than 0.2 nm from the along-track average for all band, and thus could eventually lead to consistent striping on-orbit that can be removed. For all bands, there was little to no variation of this pattern with either scan angle or polarization state. Only band M1 showed a small shift for all detectors with polarization state, and much less so for scan angle.

When these modeled band pass transmissions were applied to the Rayleigh and 2300°K blackbody radiance spectra, the results were generally small, but do span a significant range of about 1% for M1 down to about 0.3% for M7. More importantly, the resulting relative percent changes from these two spectra were anti-correlated (see the blue/red data bars in Appendix B tables). The model predicted that most of polarization response comes from the edges of the band pass. Thus, the anti-correlation was likely caused by the opposite signs of the slope for spectral shapes, which would emphasize opposite sides of the band pass. This suggests that although different source spectra may yield an overall uncertainty within 0.5%, they can still systematically disagree on a larger scale.

Conclusions

The results for the sensitivity analysis show relatively small impact. Application of an extremely unlikely, highly stressing scenarios in this study indicates that any significant uncertainty in the ocean color data products will very likely not stem from the reported uncertainty for the J1 VIIRS polarization response characterization uncertainty. However, but the analysis only accounts for impact from the uncertainty and does not account for the overall higher magnitude of the polarization sensitivity of J1 VIIRS. This would not be problem if our correction algorithm were perfect; but it is not. There are physical phenomena (e.g., aerosol scatter) that could affect TOA polarization, but would normally be treated as small and ignored. However, a greater polarization response in J1 VIIRS could magnify these effects enough to possibly impact the data quality.

Spectral effects could be a significant source of uncertainty in the polarization correction. Systematic effects arising from the spectral shape differences between the TOA spectrum and source used in tests could lead to significant additional striping. Thus it is recommended that

polarization correction coefficients used for on-orbit measurements be based on a source spectrum with a similar spectral shape to the Rayleigh spectrum.

With that caveat, and assuming that the uncertainties provided by VCST are realistic, the anomalous polarization sensitivity of the J1 VIIRS instrument is expected to a manageable issue for the production of ocean color products. Thus, approval of the waiver appears warranted. However, the realization of the potential impact of the spectral properties of polarization response merits further evaluation by the ocean color EDR or Level-2 teams. Effort should be made to understand and reduce resulting striping artifacts in the J1 VIIRS ocean color products, including exploring different test data sets to determine which minimize the effects of characterization source / atmosphere spectral shape differences.

Acknowledgments

We would like to thank NASA VCST members for their help in providing data and their analysis results from the characterization of the J1 VIIRS polarization response and Raytheon for their testing and modeling efforts of the same.

References

Brown, S.W., Eppeldauer, G.P., Lykke, K.R., (2006). Facility for spectral irradiance and radiance responsivity calibrations using uniform sources, *Applied Optics,* 45(32), pp 8218–8237.

Gordon, H., Du, T., Zhang, T., (1997). Atmospheric correction of ocean color sensors: analysis of the effects of residual instrument polarization sensitivity, *Applied Optics*, 36(27), pp 6938-6948.

Guenther, B., (2012). Validation of VIIRS Calibrations for Oceans, *Imaging and Applied Optics Technical Digest*, RM3E.3.pdf.

McIntire, J., Moyer, D., McCarthy, J.K., Brown, S.W., Lykke, K.R., De Luccia, F., Xiong, X., Butler, J.J., Guenther, B., (2011). Results from solar reflective band end-to-end testing for VIIRS F1 sensor using T-SIRCUS, *SPIE Proceedings Vol. 8153: Earth Observing Systems XVI*, James J. Butler; Xiaoxiong Xiong; Xingfa Gu, Editor(s). doi: 10.1117/12.891917.

McIntire, J., (2014). Update to Preliminary Analysis of Uncertainty in Polarization Sensitivity Analysis. NASA VCST Report Presentation. VCST_TECH_REPORT_14_013_polarization_ uncertainty.pdf, Slide 6, 25 February.

Meister, G., Kwiatkowska, E., Franz, B., Patt, F., Feldman, G., McClain, C., (2005). Moderate-Resolution Imaging Spectroradiometer ocean color polarization correction, *Applied Optics*, 44(26), pp. 5524-5535.

M1 Center Wavelength (τ weighted) (μm)

Scan Angle	Det	Polarization Angle 0°	45°	90°	135°	UNP
-55°	1	0.409501	0.409560	0.409571	0.409512	0.409535
	4	0.409587	0.409653	0.409653	0.409588	0.409619
	8	0.409595	0.409672	0.409666	0.409590	0.409630
	12	0.409480	0.409567	0.409564	0.409478	0.409521
	16	0.409255	0.409353	0.409359	0.409260	0.409306
-45°	1	0.409495	0.409558	0.409575	0.409512	0.409534
	4	0.409585	0.409656	0.409663	0.409593	0.409623
	8	0.409584	0.409664	0.409666	0.409586	0.409624
	12	0.409466	0.409557	0.409563	0.409471	0.409513
	16	0.409239	0.409340	0.409355	0.409251	0.409295
-20°	1	0.409475	0.409546	0.409578	0.409505	0.409525
	4	0.409566	0.409642	0.409665	0.409587	0.409614
	8	0.409564	0.409649	0.409668	0.409580	0.409614
	12	0.409444	0.409538	0.409561	0.409463	0.409500
	16	0.409235	0.409339	0.409372	0.409263	0.409301
-8°	1	0.409463	0.409534	0.409574	0.409500	0.409516
	4	0.409551	0.409628	0.409660	0.409580	0.409604
	8	0.409554	0.409639	0.409667	0.409577	0.409607
	12	0.409437	0.409530	0.409563	0.409464	0.409497
	16	0.409239	0.409341	0.409383	0.409275	0.409308
22°	1	0.409451	0.409521	0.409579	0.409504	0.409512
	4	0.409558	0.409633	0.409681	0.409601	0.409617
	8	0.409551	0.409631	0.409678	0.409591	0.409611
	12	0.409434	0.409520	0.409571	0.409478	0.409499
	16	0.409240	0.409335	0.409395	0.409293	0.409314
45°	1	0.409467	0.409529	0.409598	0.409529	0.409529
	4	0.409562	0.409627	0.409687	0.409615	0.409621
	8	0.409560	0.409630	0.409686	0.409610	0.409620
	12	0.409442	0.409516	0.409577	0.409496	0.409506
	16	0.409246	0.409327	0.409397	0.409308	0.409317
55°	1	0.409469	0.409527	0.409599	0.409535	0.409531
	4	0.409563	0.409623	0.409684	0.409618	0.409620
	8	0.409560	0.409623	0.409682	0.409612	0.409618
	12	0.409447	0.409514	0.409577	0.409503	0.409509
	16	0.409245	0.409320	0.409392	0.409309	0.409315

M2 Center Wavelength (τ weighted) (μm)

Scan Angle	Det	Polarization Angle 0°	45°	90°	135°	UNP
-55°	1	0.445313	0.445349	0.445338	0.445303	0.445325
	4	0.445505	0.445539	0.445541	0.445507	0.445523
	8	0.445603	0.445628	0.445647	0.445622	0.445625
	12	0.445571	0.445584	0.445616	0.445603	0.445593
	16	0.445390	0.445390	0.445433	0.445433	0.445411
-45°	1	0.445315	0.445351	0.445341	0.445307	0.445328
	4	0.445508	0.445541	0.445545	0.445511	0.445526
	8	0.445606	0.445631	0.445652	0.445626	0.445628
	12	0.445556	0.445570	0.445605	0.445590	0.445580
	16	0.445383	0.445386	0.445430	0.445427	0.445407
-20°	1	0.445309	0.445344	0.445337	0.445304	0.445323
	4	0.445498	0.445530	0.445538	0.445504	0.445517
	8	0.445594	0.445619	0.445644	0.445617	0.445618
	12	0.445552	0.445568	0.445607	0.445590	0.445579
	16	0.445375	0.445380	0.445427	0.445422	0.445400
-8°	1	0.445305	0.445339	0.445334	0.445300	0.445319
	4	0.445487	0.445520	0.445529	0.445495	0.445507
	8	0.445596	0.445622	0.445649	0.445622	0.445622
	12	0.445539	0.445555	0.445595	0.445577	0.445566
	16	0.445385	0.445391	0.445438	0.445432	0.445411
22°	1	0.445300	0.445333	0.445330	0.445297	0.445315
	4	0.445505	0.445538	0.445551	0.445517	0.445527
	8	0.445590	0.445615	0.445645	0.445617	0.445616
	12	0.445548	0.445563	0.445605	0.445588	0.445575
	16	0.445399	0.445404	0.445454	0.445448	0.445425
45°	1	0.445288	0.445320	0.445319	0.445287	0.445303
	4	0.445511	0.445542	0.445556	0.445524	0.445533
	8	0.445599	0.445622	0.445653	0.445628	0.445625
	12	0.445557	0.445570	0.445614	0.445599	0.445584
	16	0.445391	0.445395	0.445447	0.445442	0.445418
55°	1	0.445303	0.445333	0.445332	0.445302	0.445317
	4	0.445513	0.445543	0.445557	0.445526	0.445534
	8	0.445602	0.445625	0.445656	0.445631	0.445628
	12	0.445550	0.445563	0.445607	0.445593	0.445578
	16	0.445400	0.445404	0.445455	0.445451	0.445427

M4 Center Wavelength (τ weighted) (μm)

Scan Angle	Det	Polarization Angle 0°	45°	90°	135°	UNP
-55°	1	0.555492	0.555480	0.555530	0.555541	0.555511
	4	0.555769	0.555769	0.555791	0.555790	0.555780
	8	0.555937	0.555949	0.555935	0.555924	0.555936
	12	0.555922	0.555923	0.555912	0.555911	0.555917
	16	0.555693	0.555667	0.555680	0.555706	0.555686
-45°	1	0.555475	0.555475	0.555520	0.555518	0.555497
	4	0.555764	0.555771	0.555789	0.555782	0.555777
	8	0.555946	0.555959	0.555944	0.555931	0.555945
	12	0.555903	0.555906	0.555895	0.555893	0.555899
	16	0.555686	0.555659	0.555672	0.555700	0.555679
-20°	1	0.555456	0.555477	0.555513	0.555491	0.555484
	4	0.555752	0.555769	0.555785	0.555768	0.555768
	8	0.555934	0.555949	0.555937	0.555922	0.555935
	12	0.555889	0.555891	0.555882	0.555880	0.555886
	16	0.555675	0.555649	0.555662	0.555689	0.555669
-8°	1	0.555451	0.555479	0.555514	0.555485	0.555482
	4	0.555748	0.555768	0.555784	0.555763	0.555766
	8	0.555934	0.555950	0.555934	0.555918	0.555934
	12	0.555894	0.555895	0.555887	0.555885	0.555890
	16	0.555682	0.555657	0.555670	0.555696	0.555676
22°	1	0.555448	0.555488	0.555524	0.555482	0.555485
	4	0.555777	0.555803	0.555815	0.555788	0.555796
	8	0.555945	0.555962	0.555947	0.555930	0.555946
	12	0.555892	0.555894	0.555885	0.555883	0.555888
	16	0.555703	0.555680	0.555693	0.555717	0.555698
45°	1	0.555431	0.555477	0.555516	0.555468	0.555472
	4	0.555769	0.555798	0.555812	0.555782	0.555790
	8	0.555940	0.555958	0.555943	0.555925	0.555941
	12	0.555898	0.555901	0.555892	0.555890	0.555895
	16	0.555700	0.555678	0.555692	0.555716	0.555696
55°	1	0.555443	0.555490	0.555532	0.555483	0.555486
	4	0.555780	0.555810	0.555825	0.555795	0.555802
	8	0.555951	0.555969	0.555956	0.555938	0.555953
	12	0.555895	0.555898	0.555890	0.555887	0.555893
	16	0.555694	0.555671	0.555686	0.555710	0.555690

M3 Center Wavelength (τ weighted) (μm)

Scan Angle	Det	Polarization Angle 0°	45°	90°	135°	UNP
-55°	1	0.488533	0.488570	0.488551	0.488516	0.488542
	4	0.488750	0.488780	0.488778	0.488747	0.488763
	8	0.488889	0.488905	0.488920	0.488904	0.488904
	12	0.488855	0.488853	0.488879	0.488881	0.488867
	16	0.488662	0.488639	0.488671	0.488694	0.488666
-45°	1	0.488515	0.488551	0.488534	0.488500	0.488525
	4	0.488748	0.488778	0.488777	0.488746	0.488762
	8	0.488884	0.488902	0.488917	0.488899	0.488900
	12	0.488842	0.488843	0.488870	0.488868	0.488856
	16	0.488662	0.488645	0.488677	0.488694	0.488669
-20°	1	0.488508	0.488542	0.488526	0.488493	0.488517
	4	0.488736	0.488766	0.488766	0.488736	0.488751
	8	0.488874	0.488895	0.488911	0.488890	0.488892
	12	0.488829	0.488835	0.488864	0.488857	0.488846
	16	0.488650	0.488641	0.488673	0.488682	0.488661
-8°	1	0.488504	0.488537	0.488521	0.488489	0.488512
	4	0.488736	0.488766	0.488766	0.488736	0.488751
	8	0.488870	0.488891	0.488910	0.488888	0.488889
	12	0.488826	0.488834	0.488862	0.488853	0.488843
	16	0.488652	0.488646	0.488679	0.488685	0.488665
22°	1	0.488506	0.488538	0.488523	0.488492	0.488515
	4	0.488760	0.488790	0.488792	0.488763	0.488776
	8	0.488876	0.488897	0.488916	0.488894	0.488895
	12	0.488838	0.488847	0.488877	0.488868	0.488857
	16	0.488662	0.488657	0.488692	0.488697	0.488677
45°	1	0.488502	0.488534	0.488519	0.488488	0.488510
	4	0.488760	0.488790	0.488792	0.488762	0.488776
	8	0.488875	0.488896	0.488916	0.488894	0.488895
	12	0.488828	0.488837	0.488868	0.488858	0.488847
	16	0.488662	0.488657	0.488693	0.488698	0.488677
55°	1	0.488507	0.488540	0.488524	0.488493	0.488516
	4	0.488761	0.488791	0.488793	0.488763	0.488777
	8	0.488884	0.488905	0.488924	0.488902	0.488903
	12	0.488838	0.488848	0.488878	0.488868	0.488858
	16	0.488656	0.488652	0.488688	0.488692	0.488672

M5 Center Wavelength (τ weighted) (μm)

Scan Angle	Det	Polarization Angle 0°	45°	90°	135°	UNP
-55°	1	0.672034	0.671998	0.672026	0.672062	0.672030
	4	0.672332	0.672317	0.672353	0.672367	0.672342
	8	0.672473	0.672476	0.672539	0.672534	0.672505
	12	0.672370	0.672372	0.672461	0.672458	0.672415
	16	0.672086	0.672079	0.672171	0.672176	0.672128
-45°	1	0.672018	0.671992	0.672015	0.672040	0.672017
	4	0.672317	0.672307	0.672341	0.672351	0.672329
	8	0.672462	0.672464	0.672530	0.672526	0.672495
	12	0.672379	0.672372	0.672466	0.672471	0.672422
	16	0.672089	0.672071	0.672169	0.672186	0.672129
-20°	1	0.672000	0.671997	0.672011	0.672014	0.672006
	4	0.672306	0.672307	0.672338	0.672337	0.672322
	8	0.672452	0.672449	0.672519	0.672520	0.672485
	12	0.672357	0.672334	0.672440	0.672462	0.672398
	16	0.672090	0.672051	0.672155	0.672194	0.672123
-8°	1	0.671995	0.672000	0.672013	0.672008	0.672004
	4	0.672303	0.672306	0.672339	0.672335	0.672321
	8	0.672468	0.672463	0.672536	0.672539	0.672501
	12	0.672365	0.672338	0.672444	0.672471	0.672404
	16	0.672095	0.672050	0.672156	0.672202	0.672126
22°	1	0.671972	0.671992	0.672008	0.671988	0.671990
	4	0.672287	0.672295	0.672331	0.672321	0.672308
	8	0.672469	0.672459	0.672533	0.672541	0.672501
	12	0.672370	0.672332	0.672438	0.672475	0.672403
	16	0.672115	0.672057	0.672163	0.672222	0.672139
45°	1	0.671980	0.672006	0.672025	0.671999	0.672002
	4	0.672323	0.672334	0.672372	0.672360	0.672347
	8	0.672470	0.672457	0.672530	0.672541	0.672499
	12	0.672390	0.672346	0.672448	0.672492	0.672419
	16	0.672124	0.672060	0.672160	0.672226	0.672142
55°	1	0.671980	0.672008	0.672031	0.672002	0.672005
	4	0.672332	0.672344	0.672381	0.672368	0.672357
	8	0.672473	0.672459	0.672531	0.672543	0.672502
	12	0.672394	0.672348	0.672447	0.672493	0.672420
	16	0.672142	0.672077	0.672171	0.672238	0.672157

M6 Center Wavelength (τ weighted) (μm)

Scan Angle	Det	Polarization Angle 0°	45°	90°	135°	UNP
-55°	1	0.746120	0.746128	0.746128	0.746119	0.746124
	4	0.746418	0.746428	0.746428	0.746417	0.746423
	8	0.746593	0.746602	0.746596	0.746587	0.746595
	12	0.746499	0.746501	0.746488	0.746485	0.746493
	16	0.746200	0.746194	0.746174	0.746181	0.746187
-45°	1	0.746112	0.746121	0.746120	0.746111	0.746116
	4	0.746414	0.746425	0.746424	0.746413	0.746419
	8	0.746591	0.746600	0.746595	0.746585	0.746593
	12	0.746497	0.746499	0.746486	0.746484	0.746492
	16	0.746192	0.746185	0.746166	0.746173	0.746179
-20°	1	0.746104	0.746115	0.746114	0.746104	0.746109
	4	0.746409	0.746421	0.746420	0.746409	0.746415
	8	0.746583	0.746592	0.746587	0.746577	0.746585
	12	0.746493	0.746495	0.746482	0.746481	0.746488
	16	0.746202	0.746194	0.746177	0.746185	0.746189
-8°	1	0.746098	0.746109	0.746108	0.746098	0.746103
	4	0.746402	0.746413	0.746413	0.746401	0.746407
	8	0.746595	0.746604	0.746599	0.746590	0.746597
	12	0.746490	0.746491	0.746479	0.746478	0.746484
	16	0.746208	0.746200	0.746183	0.746192	0.746196
22°	1	0.746085	0.746096	0.746096	0.746085	0.746091
	4	0.746401	0.746412	0.746413	0.746401	0.746407
	8	0.746595	0.746602	0.746598	0.746591	0.746596
	12	0.746489	0.746487	0.746476	0.746478	0.746482
	16	0.746219	0.746208	0.746192	0.746203	0.746206
45°	1	0.746094	0.746105	0.746106	0.746095	0.746100
	4	0.746442	0.746453	0.746455	0.746443	0.746448
	8	0.746596	0.746603	0.746599	0.746592	0.746597
	12	0.746502	0.746499	0.746487	0.746490	0.746494
	16	0.746219	0.746207	0.746190	0.746203	0.746205
55°	1	0.746084	0.746096	0.746096	0.746085	0.746090
	4	0.746435	0.746447	0.746448	0.746437	0.746442
	8	0.746593	0.746600	0.746595	0.746589	0.746594
	12	0.746499	0.746496	0.746484	0.746488	0.746492
	16	0.746225	0.746212	0.746196	0.746208	0.746210

M7 Center Wavelength (τ weighted) (μm)

Scan Angle	Det	Polarization Angle 0°	45°	90°	135°	UNP
-55°	1	0.864743	0.864754	0.864775	0.864764	0.864759
	4	0.865133	0.865144	0.865154	0.865143	0.865143
	8	0.865347	0.865362	0.865354	0.865339	0.865350
	12	0.865273	0.865295	0.865263	0.865240	0.865268
	16	0.864945	0.864977	0.864918	0.864885	0.864931
-45°	1	0.864739	0.864747	0.864764	0.864757	0.864752
	4	0.865117	0.865127	0.865134	0.865124	0.865125
	8	0.865335	0.865350	0.865339	0.865323	0.865337
	12	0.865265	0.865288	0.865251	0.865227	0.865258
	16	0.864952	0.864984	0.864922	0.864889	0.864937
-20°	1	0.864716	0.864720	0.864733	0.864729	0.864725
	4	0.865100	0.865108	0.865110	0.865102	0.865105
	8	0.865318	0.865332	0.865317	0.865302	0.865317
	12	0.865243	0.865266	0.865224	0.865201	0.865234
	16	0.864929	0.864960	0.864894	0.864863	0.864912
-8°	1	0.864716	0.864720	0.864731	0.864727	0.864724
	4	0.865114	0.865123	0.865123	0.865114	0.865119
	8	0.865344	0.865360	0.865341	0.865325	0.865342
	12	0.865267	0.865289	0.865246	0.865223	0.865256
	16	0.864940	0.864970	0.864903	0.864873	0.864921
22°	1	0.864707	0.864711	0.864721	0.864717	0.864714
	4	0.865117	0.865125	0.865123	0.865116	0.865120
	8	0.865338	0.865352	0.865332	0.865318	0.865335
	12	0.865263	0.865284	0.865240	0.865219	0.865251
	16	0.864966	0.864992	0.864924	0.864897	0.864945
45°	1	0.864720	0.864726	0.864735	0.864729	0.864727
	4	0.865151	0.865160	0.865157	0.865147	0.865154
	8	0.865351	0.865365	0.865344	0.865330	0.865347
	12	0.865274	0.865294	0.865247	0.865227	0.865260
	16	0.864958	0.864983	0.864912	0.864887	0.864935
55°	1	0.864723	0.864730	0.864739	0.864733	0.864731
	4	0.865159	0.865169	0.865166	0.865156	0.865162
	8	0.865353	0.865368	0.865346	0.865331	0.865350
	12	0.865276	0.865296	0.865249	0.865229	0.865262
	16	0.864966	0.864991	0.864919	0.864894	0.864943

Table A – Band Centroid. provide band pass centroid based on the FRED model spectral transmission as a function of detector, scan angle, and polarization angle (UNP = unpolarized). Cells are colored on a scale from orange to yellow, such that yellow corresponds to the maximum for the band and orange the minimum.

APPENDIX B – Radiance Percent Difference by Source Spectra

Table B.1

M1 Relative Change in Rayleigh Radiance (%)

Scan Angle	Det	Polarization Angle 0°	45°	90°	135°	UNP
-55°	1	0.02	-0.06	-0.07	0.01	-0.02
	4	-0.06	-0.14	-0.15	-0.07	-0.10
	8	-0.07	-0.15	-0.16	-0.07	-0.11
	12	0.05	-0.04	-0.05	0.04	0.00
	16	0.27	0.17	0.15	0.25	0.21
-45°	1	0.02	-0.06	-0.07	0.01	-0.02
	4	-0.06	-0.15	-0.15	-0.07	-0.11
	8	-0.06	-0.15	-0.16	-0.07	-0.10
	12	0.06	-0.03	-0.05	0.04	0.00
	16	0.28	0.18	0.15	0.26	0.22
-20°	1	0.04	-0.04	-0.07	0.02	-0.01
	4	-0.04	-0.13	-0.16	-0.06	-0.10
	8	-0.04	-0.13	-0.16	-0.06	-0.10
	12	0.08	-0.02	-0.05	0.05	0.02
	16	0.29	0.18	0.14	0.24	0.21
-8°	1	0.06	-0.03	-0.07	0.02	0.00
	4	-0.03	-0.12	-0.15	-0.06	-0.09
	8	-0.03	-0.12	-0.16	-0.06	-0.09
	12	0.09	-0.01	-0.05	0.05	0.02
	16	0.28	0.18	0.13	0.23	0.21
22°	1	0.07	-0.02	-0.07	0.02	0.00
	4	-0.03	-0.12	-0.17	-0.08	-0.10
	8	-0.02	-0.11	-0.17	-0.07	-0.09
	12	0.09	0.00	-0.06	0.04	0.02
	16	0.28	0.19	0.11	0.21	0.20
45°	1	0.05	-0.03	-0.09	-0.01	-0.02
	4	-0.04	-0.12	-0.18	-0.09	-0.10
	8	-0.03	-0.11	-0.18	-0.09	-0.10
	12	0.08	0.01	-0.07	0.02	0.01
	16	0.28	0.20	0.11	0.20	0.20
55°	1	0.05	-0.03	-0.09	-0.01	-0.02
	4	-0.04	-0.11	-0.18	-0.10	-0.10
	8	-0.03	-0.11	-0.17	-0.09	-0.10
	12	0.08	0.01	-0.07	0.01	0.01
	16	0.28	0.20	0.12	0.20	0.20

M1 Relative Change in Blackbody Radiance (%)

Polarization Angle 0°	45°	90°	135°	UNP
0.03	0.05	0.09	0.01	0.03
0.20	0.30	0.29	0.20	0.25
0.24	0.38	0.34	0.19	0.29
0.05	0.15	0.09	0.10	0.02
0.61	0.36	0.40	0.65	0.51
0.04	0.04	0.10	0.01	0.03
0.20	0.31	0.32	0.21	0.26
0.21	0.36	0.34	0.18	0.27
0.08	0.12	0.09	0.12	0.00
0.65	0.39	0.42	0.67	0.53
0.09	0.01	0.11	0.00	0.01
0.15	0.28	0.33	0.20	0.23
0.16	0.32	0.34	0.17	0.24
0.14	0.08	0.09	0.14	0.03
0.66	0.40	0.37	0.64	0.52
0.12	0.02	0.10	0.02	0.02
0.12	0.24	0.31	0.18	0.21
0.13	0.30	0.34	0.16	0.23
0.15	0.06	0.09	0.13	0.04
0.65	0.39	0.34	0.61	0.50
0.15	0.05	0.11	0.01	0.03
0.13	0.26	0.36	0.23	0.24
0.13	0.29	0.36	0.19	0.24
0.16	0.03	0.11	0.10	0.03
0.65	0.41	0.31	0.57	0.49
0.11	0.03	0.16	0.06	0.02
0.14	0.25	0.38	0.26	0.25
0.15	0.28	0.39	0.24	0.26
0.14	0.02	0.12	0.06	0.02
0.63	0.43	0.31	0.53	0.48
0.11	0.03	0.16	0.07	0.02
0.14	0.23	0.37	0.27	0.25
0.15	0.27	0.38	0.25	0.26
0.13	0.02	0.13	0.04	0.01
0.63	0.44	0.32	0.53	0.49

Table B.2

M2 Relative Change in Rayleigh Radiance (%)

Scan Angle	Det	Polarization Angle 0°	45°	90°	135°	UNP
-55°	1	0.17	0.12	0.13	0.18	0.15
	4	-0.01	-0.05	-0.05	-0.01	-0.03
	8	-0.09	-0.12	-0.15	-0.12	-0.12
	12	-0.07	-0.08	-0.12	-0.10	-0.09
	16	0.10	0.10	0.05	0.05	0.07
-45°	1	0.16	0.12	0.13	0.17	0.15
	4	-0.01	-0.05	-0.05	-0.01	-0.03
	8	-0.10	-0.13	-0.15	-0.12	-0.12
	12	-0.05	-0.07	-0.11	-0.09	-0.08
	16	0.10	0.10	0.05	0.05	0.08
-20°	1	0.17	0.13	0.13	0.18	0.15
	4	0.00	-0.04	-0.05	-0.01	-0.02
	8	-0.09	-0.12	-0.14	-0.11	-0.11
	12	-0.05	-0.06	-0.11	-0.09	-0.08
	16	0.11	0.11	0.05	0.06	0.08
-8°	1	0.17	0.13	0.14	0.18	0.16
	4	0.01	-0.03	-0.04	0.00	-0.01
	8	-0.09	-0.12	-0.15	-0.12	-0.12
	12	-0.04	-0.05	-0.10	-0.08	-0.07
	16	0.10	0.10	0.04	0.05	0.07
22°	1	0.18	0.13	0.14	0.18	0.16
	4	-0.01	-0.05	-0.06	-0.02	-0.03
	8	-0.08	-0.11	-0.14	-0.11	-0.11
	12	-0.04	-0.06	-0.11	-0.09	-0.07
	16	0.09	0.09	0.03	0.03	0.06
45°	1	0.19	0.15	0.15	0.19	0.17
	4	-0.01	-0.05	-0.06	-0.02	-0.04
	8	-0.09	-0.12	-0.15	-0.12	-0.12
	12	-0.05	-0.07	-0.12	-0.10	-0.08
	16	0.10	0.09	0.04	0.04	0.07
55°	1	0.17	0.13	0.14	0.18	0.16
	4	-0.01	-0.05	-0.06	-0.03	-0.04
	8	-0.09	-0.12	-0.15	-0.12	-0.12
	12	-0.05	-0.06	-0.11	-0.09	-0.08
	16	0.09	0.09	0.03	0.03	0.06

M2 Relative Change in Blackbody Radiance (%)

Polarization Angle 0°	45°	90°	135°	UNP
-0.35	-0.31	-0.33	-0.36	-0.34
0.04	0.08	0.08	0.04	0.06
0.24	0.27	0.29	0.26	0.27
0.18	0.19	0.23	0.21	0.20
-0.19	-0.18	-0.13	-0.14	-0.16
-0.35	-0.31	-0.32	-0.35	-0.33
0.05	0.08	0.09	0.05	0.07
0.25	0.28	0.30	0.27	0.27
0.15	0.17	0.21	0.19	0.18
-0.21	-0.19	-0.13	-0.15	-0.17
-0.36	-0.32	-0.33	-0.36	-0.34
0.03	0.06	0.07	0.04	0.05
0.22	0.25	0.29	0.25	0.25
0.14	0.16	0.22	0.19	0.18
-0.22	-0.21	-0.14	-0.16	-0.18
-0.37	-0.33	-0.33	-0.37	-0.35
0.00	0.04	0.06	0.02	0.03
0.23	0.26	0.30	0.26	0.26
0.11	0.14	0.19	0.16	0.15
-0.20	-0.18	-0.12	-0.14	-0.16
-0.38	-0.35	-0.34	-0.37	-0.36
0.04	0.08	0.10	0.06	0.07
0.22	0.25	0.29	0.25	0.25
0.13	0.15	0.21	0.18	0.17
-0.18	-0.16	-0.09	-0.11	-0.13
-0.40	-0.37	-0.36	-0.39	-0.38
0.05	0.09	0.11	0.08	0.08
0.23	0.26	0.31	0.28	0.27
0.15	0.17	0.23	0.21	0.19
-0.19	-0.18	-0.10	-0.12	-0.15
-0.37	-0.35	-0.34	-0.36	-0.35
0.06	0.09	0.11	0.08	0.08
0.24	0.27	0.31	0.28	0.27
0.13	0.15	0.22	0.19	0.17
-0.17	-0.16	-0.08	-0.10	-0.13

Table B.3

M3 Relative Change in Rayleigh Radiance (%)

Scan Angle	Det	Polarization Angle 0°	45°	90°	135°	UNP
-55°	1	0.17	0.13	0.15	0.19	0.16
	4	0.00	-0.04	-0.03	0.00	-0.02
	8	-0.12	-0.14	-0.15	-0.13	-0.13
	12	-0.09	-0.09	-0.12	-0.12	-0.10
	16	0.07	0.09	0.06	0.03	0.06
-45°	1	0.19	0.15	0.17	0.20	0.18
	4	0.00	-0.03	-0.03	0.00	-0.02
	8	-0.11	-0.13	-0.15	-0.13	-0.13
	12	-0.08	-0.08	-0.11	-0.11	-0.09
	16	0.07	0.08	0.05	0.03	0.06
-20°	1	0.19	0.16	0.17	0.21	0.18
	4	0.01	-0.02	-0.02	0.01	-0.01
	8	-0.10	-0.13	-0.14	-0.12	-0.12
	12	-0.07	-0.07	-0.10	-0.10	-0.09
	16	0.08	0.09	0.05	0.04	0.07
-8°	1	0.20	0.16	0.18	0.21	0.19
	4	0.01	-0.02	-0.02	0.01	-0.01
	8	-0.10	-0.12	-0.14	-0.12	-0.12
	12	-0.07	-0.07	-0.10	-0.10	-0.08
	16	0.08	0.08	0.05	0.04	0.06
22°	1	0.20	0.16	0.18	0.21	0.19
	4	-0.01	-0.04	-0.05	-0.01	-0.03
	8	-0.11	-0.13	-0.15	-0.13	-0.13
	12	-0.08	-0.08	-0.12	-0.11	-0.10
	16	0.07	0.07	0.04	0.03	0.05
45°	1	0.20	0.16	0.18	0.21	0.19
	4	-0.01	-0.04	-0.05	-0.01	-0.03
	8	-0.11	-0.13	-0.15	-0.12	-0.13
	12	-0.07	-0.08	-0.11	-0.10	-0.09
	16	0.07	0.07	0.04	0.03	0.05
55°	1	0.19	0.16	0.18	0.21	0.19
	4	-0.01	-0.04	-0.05	-0.01	-0.03
	8	-0.11	-0.13	-0.15	-0.13	-0.13
	12	-0.08	-0.08	-0.12	-0.11	-0.10
	16	0.07	0.08	0.04	0.03	0.06

M3 Relative Change in Blackbody Radiance (%)

Polarization Angle 0°	45°	90°	135°	UNP
-0.33	-0.28	-0.31	-0.35	-0.32
0.02	0.05	0.05	0.02	0.04
0.24	0.26	0.28	0.26	0.26
0.19	0.18	0.21	0.22	0.20
-0.12	-0.15	-0.12	-0.09	-0.12
-0.35	-0.31	-0.33	-0.37	-0.34
0.02	0.05	0.05	0.02	0.03
0.24	0.25	0.27	0.25	0.25
0.17	0.17	0.20	0.20	0.18
-0.12	-0.14	-0.11	-0.09	-0.11
-0.37	-0.33	-0.35	-0.38	-0.36
0.00	0.03	0.03	0.00	0.02
0.22	0.24	0.26	0.24	0.24
0.15	0.16	0.19	0.18	0.17
-0.14	-0.15	-0.11	-0.10	-0.13
-0.37	-0.34	-0.35	-0.39	-0.36
0.00	0.03	0.03	0.00	0.01
0.21	0.24	0.26	0.23	0.24
0.14	0.15	0.18	0.17	0.16
-0.14	-0.14	-0.10	-0.10	-0.12
-0.37	-0.34	-0.35	-0.38	-0.36
0.04	0.07	0.07	0.04	0.06
0.22	0.25	0.27	0.24	0.25
0.16	0.17	0.21	0.20	0.18
-0.12	-0.12	-0.08	-0.08	-0.10
-0.38	-0.34	-0.36	-0.39	-0.37
0.04	0.07	0.07	0.04	0.06
0.22	0.25	0.27	0.24	0.24
0.14	0.16	0.19	0.18	0.17
-0.12	-0.12	-0.08	-0.08	-0.10
-0.37	-0.33	-0.35	-0.38	-0.36
0.04	0.07	0.08	0.04	0.06
0.23	0.26	0.28	0.26	0.26
0.16	0.17	0.21	0.20	0.19
-0.13	-0.13	-0.09	-0.09	-0.11

Table B.4

M4 Relative Change in Rayleigh Radiance (%)

Scan Angle	Det	Polarization Angle 0°	45°	90°	135°	UNP
-55°	1	0.20	0.20	0.16	0.16	0.18
	4	0.00	-0.01	-0.03	-0.02	-0.02
	8	-0.13	-0.14	-0.13	-0.12	-0.13
	12	-0.11	-0.12	-0.12	-0.11	-0.11
	16	0.05	0.07	0.05	0.04	0.05
-45°	1	0.21	0.20	0.17	0.18	0.19
	4	0.00	-0.01	-0.03	-0.01	-0.01
	8	-0.13	-0.15	-0.14	-0.12	-0.13
	12	-0.10	-0.11	-0.10	-0.10	-0.10
	16	0.06	0.08	0.06	0.04	0.06
-20°	1	0.22	0.20	0.17	0.20	0.20
	4	0.01	-0.01	-0.02	0.00	-0.01
	8	-0.12	-0.14	-0.13	-0.12	-0.13
	12	-0.09	-0.09	-0.09	-0.09	-0.09
	16	0.06	0.08	0.07	0.05	0.06
-8°	1	0.23	0.20	0.17	0.20	0.20
	4	0.01	-0.01	-0.02	0.00	-0.01
	8	-0.12	-0.14	-0.13	-0.11	-0.13
	12	-0.09	-0.10	-0.10	-0.09	-0.10
	16	0.06	0.08	0.06	0.04	0.06
22°	1	0.23	0.19	0.17	0.21	0.20
	4	-0.01	-0.04	-0.05	-0.02	-0.03
	8	-0.13	-0.15	-0.14	-0.12	-0.14
	12	-0.09	-0.10	-0.09	-0.09	-0.09
	16	0.04	0.06	0.05	0.03	0.04
45°	1	0.24	0.20	0.17	0.22	0.21
	4	0.00	-0.03	-0.04	-0.01	-0.02
	8	-0.13	-0.14	-0.14	-0.12	-0.13
	12	-0.10	-0.10	-0.10	-0.10	-0.10
	16	0.04	0.06	0.05	0.03	0.05
55°	1	0.23	0.19	0.16	0.21	0.20
	4	-0.01	-0.04	-0.05	-0.02	-0.03
	8	-0.13	-0.15	-0.15	-0.13	-0.14
	12	-0.10	-0.10	-0.10	-0.09	-0.10
	16	0.05	0.07	0.05	0.03	0.05

M4 Relative Change in Blackbody Radiance (%)

Polarization Angle 0°	45°	90°	135°	UNP
-0.30	-0.32	-0.26	-0.24	-0.28
0.02	0.01	0.03	0.04	0.02
0.20	0.21	0.19	0.19	0.20
0.19	0.19	0.17	0.17	0.18
-0.07	-0.10	-0.09	-0.06	-0.08
-0.31	-0.32	-0.27	-0.26	-0.29
0.01	0.01	0.03	0.03	0.02
0.21	0.22	0.20	0.19	0.21
0.17	0.17	0.15	0.15	0.16
-0.08	-0.11	-0.10	-0.07	-0.09
-0.34	-0.32	-0.28	-0.29	-0.31
0.00	0.01	0.02	0.01	0.01
0.20	0.21	0.19	0.18	0.20
0.15	0.15	0.13	0.13	0.14
-0.09	-0.12	-0.11	-0.08	-0.10
-0.34	-0.32	-0.28	-0.30	-0.31
-0.01	0.01	0.02	0.01	0.01
0.20	0.21	0.19	0.18	0.20
0.16	0.16	0.14	0.14	0.15
-0.08	-0.11	-0.10	-0.08	-0.09
-0.34	-0.31	-0.27	-0.30	-0.31
0.03	0.05	0.06	0.04	0.04
0.21	0.23	0.21	0.19	0.21
0.15	0.15	0.14	0.14	0.15
-0.06	-0.08	-0.08	-0.05	-0.07
-0.36	-0.32	-0.28	-0.32	-0.32
0.02	0.04	0.05	0.03	0.03
0.21	0.22	0.20	0.19	0.20
0.16	0.16	0.15	0.14	0.15
-0.06	-0.09	-0.08	-0.05	-0.07
-0.35	-0.31	-0.26	-0.30	-0.30
0.03	0.05	0.07	0.04	0.05
0.22	0.23	0.22	0.20	0.22
0.16	0.16	0.14	0.14	0.15
-0.07	-0.09	-0.08	-0.06	-0.08

Table B.5

M5 Relative Change in Rayleigh Radiance (%)

Scan Angle	Det	Polarization Angle 0°	45°	90°	135°	UNP
-55°	1	0.14	0.17	0.15	0.13	0.15
	4	-0.03	-0.02	-0.05	-0.05	-0.04
	8	-0.12	-0.12	-0.16	-0.15	-0.14
	12	-0.05	-0.06	-0.11	-0.11	-0.08
	16	0.11	0.12	0.06	0.06	0.09
-45°	1	0.15	0.17	0.16	0.14	0.16
	4	-0.02	-0.02	-0.04	-0.04	-0.03
	8	-0.11	-0.11	-0.15	-0.15	-0.13
	12	-0.06	-0.06	-0.11	-0.12	-0.09
	16	0.11	0.12	0.06	0.05	0.09
-20°	1	0.17	0.17	0.16	0.16	0.16
	4	-0.02	-0.02	-0.04	-0.04	-0.03
	8	-0.10	-0.10	-0.15	-0.14	-0.12
	12	-0.05	-0.03	-0.10	-0.11	-0.07
	16	0.11	0.14	0.07	0.05	0.09
-8°	1	0.17	0.16	0.16	0.16	0.16
	4	-0.01	-0.02	-0.04	-0.03	-0.03
	8	-0.11	-0.11	-0.16	-0.16	-0.13
	12	-0.05	-0.04	-0.10	-0.12	-0.08
	16	0.11	0.14	0.07	0.04	0.09
22°	1	0.18	0.17	0.16	0.18	0.17
	4	-0.01	-0.01	-0.03	-0.03	-0.02
	8	-0.11	-0.11	-0.15	-0.16	-0.13
	12	-0.06	-0.03	-0.10	-0.12	-0.08
	16	0.10	0.13	0.07	0.03	0.08
45°	1	0.18	0.16	0.15	0.17	0.16
	4	-0.03	-0.04	-0.06	-0.05	-0.04
	8	-0.11	-0.11	-0.15	-0.16	-0.13
	12	-0.07	-0.04	-0.10	-0.13	-0.08
	16	0.09	0.13	0.07	0.03	0.08
55°	1	0.18	0.16	0.15	0.17	0.16
	4	-0.03	-0.04	-0.06	-0.05	-0.05
	8	-0.12	-0.11	-0.15	-0.16	-0.13
	12	-0.07	-0.04	-0.10	-0.13	-0.09
	16	0.08	0.12	0.07	0.02	0.07

M5 Relative Change in Blackbody Radiance (%)

Polarization Angle 0°	45°	90°	135°	UNP
-0.16	-0.18	-0.16	-0.14	-0.16
0.04	0.03	0.05	0.06	0.04
0.13	0.13	0.17	0.16	0.15
0.06	0.06	0.12	0.12	0.09
-0.12	-0.13	-0.07	-0.06	-0.10
-0.17	-0.18	-0.17	-0.15	-0.17
0.03	0.02	0.04	0.05	0.03
0.12	0.12	0.16	0.16	0.14
0.07	0.06	0.12	0.12	0.09
-0.12	-0.13	-0.07	-0.06	-0.09
-0.18	-0.18	-0.17	-0.17	-0.17
0.02	0.02	0.04	0.04	0.03
0.11	0.11	0.15	0.16	0.13
0.05	0.04	0.10	0.12	0.08
-0.12	-0.14	-0.08	-0.05	-0.10
-0.18	-0.18	-0.17	-0.17	-0.17
0.02	0.02	0.04	0.04	0.03
0.12	0.12	0.17	0.17	0.14
0.06	0.04	0.11	0.12	0.08
-0.12	-0.14	-0.08	-0.05	-0.10
-0.19	-0.18	-0.17	-0.18	-0.18
0.01	0.01	0.03	0.03	0.02
0.12	0.12	0.16	0.17	0.14
0.06	0.04	0.10	0.13	0.08
-0.10	-0.14	-0.07	-0.04	-0.09
-0.19	-0.17	-0.16	-0.18	-0.18
0.03	0.04	0.06	0.05	0.04
0.12	0.12	0.16	0.17	0.14
0.07	0.04	0.11	0.14	0.09
-0.10	-0.14	-0.07	-0.03	-0.09
-0.19	-0.17	-0.16	-0.18	-0.17
0.04	0.04	0.07	0.06	0.05
0.13	0.12	0.16	0.17	0.14
0.07	0.05	0.11	0.14	0.09
-0.09	-0.13	-0.07	-0.03	-0.08

Table B.6

M6 Relative Change in Rayleigh Radiance (%)

Scan Angle	Det	Polarization Angle 0°	45°	90°	135°	UNP
-55°	1	0.13	0.13	0.13	0.13	0.13
	4	-0.03	-0.04	-0.04	-0.03	-0.03
	8	-0.12	-0.13	-0.13	-0.12	-0.13
	12	-0.07	-0.08	-0.07	-0.07	-0.07
	16	0.09	0.09	0.10	0.10	0.09
-45°	1	0.13	0.13	0.13	0.13	0.13
	4	-0.03	-0.03	-0.03	-0.03	-0.03
	8	-0.12	-0.13	-0.13	-0.12	-0.12
	12	-0.07	-0.07	-0.07	-0.07	-0.07
	16	0.09	0.09	0.10	0.10	0.10
-20°	1	0.14	0.13	0.13	0.14	0.14
	4	-0.03	-0.03	-0.03	-0.03	-0.03
	8	-0.12	-0.12	-0.12	-0.12	-0.12
	12	-0.07	-0.07	-0.06	-0.06	-0.07
	16	0.09	0.09	0.10	0.09	0.09
-8°	1	0.14	0.14	0.14	0.14	0.14
	4	-0.02	-0.03	-0.03	-0.02	-0.02
	8	-0.13	-0.13	-0.13	-0.12	-0.13
	12	-0.07	-0.07	-0.06	-0.06	-0.07
	16	0.08	0.09	0.10	0.09	0.09
22°	1	0.15	0.14	0.14	0.15	0.15
	4	-0.02	-0.03	-0.03	-0.02	-0.02
	8	-0.13	-0.13	-0.13	-0.12	-0.13
	12	-0.07	-0.07	-0.06	-0.06	-0.06
	16	0.08	0.08	0.09	0.08	0.08
45°	1	0.14	0.14	0.14	0.14	0.14
	4	-0.04	-0.05	-0.05	-0.04	-0.05
	8	-0.13	-0.13	-0.13	-0.12	-0.13
	12	-0.08	-0.07	-0.07	-0.07	-0.07
	16	0.08	0.08	0.09	0.09	0.08
55°	1	0.15	0.14	0.14	0.15	0.15
	4	-0.04	-0.05	-0.05	-0.04	-0.04
	8	-0.12	-0.13	-0.13	-0.12	-0.13
	12	-0.07	-0.07	-0.07	-0.07	-0.07
	16	0.07	0.08	0.09	0.08	0.08

M6 Relative Change in Blackbody Radiance (%)

Polarization Angle 0°	45°	90°	135°	UNP
-0.11	-0.11	-0.11	-0.11	-0.11
0.03	0.03	0.03	0.03	0.03
0.10	0.11	0.11	0.10	0.11
0.06	0.06	0.06	0.06	0.06
-0.07	-0.08	-0.08	-0.08	-0.08
-0.11	-0.11	-0.11	-0.11	-0.11
0.02	0.03	0.03	0.02	0.03
0.10	0.11	0.11	0.10	0.10
0.06	0.06	0.06	0.06	0.06
-0.08	-0.08	-0.09	-0.09	-0.08
-0.12	-0.11	-0.11	-0.12	-0.11
0.02	0.03	0.03	0.02	0.02
0.10	0.10	0.10	0.10	0.10
0.06	0.06	0.05	0.05	0.06
-0.07	-0.08	-0.08	-0.08	-0.08
-0.12	-0.11	-0.11	-0.12	-0.12
0.02	0.02	0.02	0.02	0.02
0.11	0.11	0.11	0.10	0.11
0.06	0.06	0.05	0.05	0.06
-0.07	-0.07	-0.08	-0.08	-0.08
-0.13	-0.12	-0.12	-0.13	-0.12
0.02	0.02	0.02	0.02	0.02
0.11	0.11	0.11	0.10	0.11
0.06	0.06	0.05	0.05	0.05
-0.06	-0.07	-0.08	-0.07	-0.07
-0.12	-0.12	-0.12	-0.12	-0.12
0.04	0.04	0.04	0.04	0.04
0.11	0.11	0.11	0.10	0.11
0.06	0.06	0.06	0.06	0.06
-0.06	-0.07	-0.08	-0.07	-0.07
-0.13	-0.12	-0.12	-0.13	-0.12
0.03	0.04	0.04	0.03	0.04
0.11	0.11	0.11	0.10	0.11
0.06	0.06	0.06	0.06	0.06
-0.06	-0.07	-0.08	-0.07	-0.07

Table B.7

M7 Relative Change in Rayleigh Radiance (%)

Scan Angle	Det	Polarization Angle				
		0°	45°	90°	135°	UNP
-55°	1	0.16	0.15	0.14	0.15	0.15
	4	-0.02	-0.03	-0.04	-0.03	-0.03
	8	-0.12	-0.13	-0.13	-0.12	-0.13
	12	-0.09	-0.10	-0.09	-0.08	-0.09
	16	0.06	0.05	0.08	0.09	0.07
-45°	1	0.16	0.15	0.15	0.15	0.15
	4	-0.02	-0.02	-0.03	-0.02	-0.02
	8	-0.12	-0.13	-0.12	-0.11	-0.12
	12	-0.09	-0.10	-0.08	-0.07	-0.08
	16	0.06	0.04	0.07	0.09	0.07
-20°	1	0.17	0.16	0.16	0.16	0.16
	4	-0.01	-0.01	-0.02	-0.01	-0.01
	8	-0.11	-0.12	-0.11	-0.10	-0.11
	12	-0.08	-0.09	-0.07	-0.06	-0.07
	16	0.07	0.05	0.09	0.10	0.08
-8°	1	0.17	0.16	0.16	0.16	0.16
	4	-0.02	-0.02	-0.02	-0.02	-0.02
	8	-0.12	-0.13	-0.12	-0.11	-0.12
	12	-0.09	-0.10	-0.08	-0.07	-0.08
	16	0.06	0.05	0.08	0.10	0.07
22°	1	0.17	0.17	0.17	0.17	0.17
	4	-0.02	-0.02	-0.02	-0.02	-0.02
	8	-0.12	-0.13	-0.12	-0.11	-0.12
	12	-0.09	-0.10	-0.07	-0.06	-0.08
	16	0.05	0.04	0.07	0.08	0.06
45°	1	0.17	0.16	0.16	0.16	0.16
	4	-0.03	-0.04	-0.04	-0.03	-0.03
	8	-0.13	-0.13	-0.12	-0.12	-0.12
	12	-0.09	-0.10	-0.08	-0.07	-0.08
	16	0.06	0.04	0.08	0.09	0.07
55°	1	0.17	0.16	0.16	0.16	0.16
	4	-0.04	-0.04	-0.04	-0.03	-0.04
	8	-0.13	-0.13	-0.12	-0.12	-0.13
	12	-0.09	-0.10	-0.08	-0.07	-0.09
	16	0.05	0.04	0.07	0.09	0.06

M7 Relative Change in Blackbody Radiance (%)

Polarization Angle				
0°	45°	90°	135°	UNP
-0.09	-0.08	-0.08	-0.08	-0.08
0.01	0.02	0.02	0.02	0.02
0.07	0.07	0.07	0.07	0.07
0.05	0.06	0.05	0.04	0.05
-0.03	-0.03	-0.04	-0.05	-0.04
-0.09	-0.09	-0.08	-0.08	-0.08
0.01	0.01	0.01	0.01	0.01
0.07	0.07	0.07	0.06	0.07
0.05	0.05	0.04	0.04	0.05
-0.03	-0.02	-0.04	-0.05	-0.04
-0.09	-0.09	-0.09	-0.09	-0.09
0.01	0.01	0.01	0.01	0.01
0.06	0.07	0.06	0.06	0.06
0.04	0.05	0.04	0.03	0.04
-0.04	-0.03	-0.05	-0.06	-0.04
-0.09	-0.09	-0.09	-0.09	-0.09
0.01	0.01	0.01	0.01	0.01
0.07	0.07	0.07	0.06	0.07
0.05	0.05	0.04	0.04	0.05
-0.04	-0.03	-0.05	-0.05	-0.04
-0.10	-0.09	-0.09	-0.09	-0.09
0.01	0.01	0.01	0.01	0.01
0.07	0.07	0.07	0.06	0.07
0.05	0.05	0.04	0.04	0.04
-0.03	-0.02	-0.04	-0.05	-0.03
-0.09	-0.09	-0.09	-0.09	-0.09
0.02	0.02	0.02	0.02	0.02
0.07	0.07	0.07	0.06	0.07
0.05	0.06	0.04	0.04	0.05
-0.03	-0.02	-0.04	-0.05	-0.04
-0.09	-0.09	-0.09	-0.09	-0.09
0.02	0.02	0.02	0.02	0.02
0.07	0.07	0.07	0.07	0.07
0.05	0.06	0.04	0.04	0.05
-0.03	-0.02	-0.04	-0.05	-0.04